Signature of functional enzyme dynamics in quasielastic neutron scattering spectra: The case of Phosphoglycerate Kinase

Abir N. Hassani[1,2,3], Luman Haris[3,4], Markus Appel[5], Tilo Seydel[5], Andreas M. Stadler[3,4] *, and Gerald R. Kneller[1,2†]

[1] *Centre de Biophysique Moléculaire, CNRS and Univ. d'Orléans; Rue Charles Sadron, 45071 Orléans, France*

[2] *Synchrotron Soleil; L'Orme de Merisiers, 91192 Gif-sur-Yvette, France*

[3] *Jülich Centre for Neutron Science (JCNS-1) and Institute of Biological Information Processing (IBI-8), Forschungszentrum Jülich GmbH, 52425 Jülich, Germany,*

[4] *Institute of Physical Chemistry, RWTH Aachen University, Landoltweg 2, 52056 Aachen, Germany and*

[5] *Institut Laue Langevin, 71 Avenue des Martyrs, 38042 Grenoble Cedex 9, France*

We present an analysis of high-resolution quasi-elastic neutron scattering spectra of phosphoglycerate kinase which elucidates the influence of the enzymatic activity on the dynamics of the protein. We show that in the active state the inter-domain motions are amplified and the intra-domain asymptotic power-law relaxation $\propto t^{-\alpha}$ is accelerated, with a reduced coefficient α. Employing an energy landscape picture of protein dynamics, this observation can be translated into a widening of the distribution of energy barriers separating conformational substates of the protein.

Understanding the functional dynamics of enzymes is a fundamental issue in molecular biophysics, biology, and biochemistry. Phosphoglycerate kinase (PGK) is one example for which the dynamics-function relationship has been intensively studied with various methods, including structural NMR, X-ray crystallography, quasielastic neutron scattering (QENS), neutron spin echo (NSE) spectroscopy, and Molecular Dynamics (MD) simulation [1–10]. PGK is a monomeric enzyme which is fundamental for the metabolism of all living organisms. By converting 1,3-bisphosphoglycerate to 3-phosphoglycerate it catalyzes one of the two ATP-producing reactions of the glycolytic pathway and it participates also in gluconeogenesis by catalyzing the opposite reaction to produce 1,3- bisphosphoglycerate and ADP [11],

$$\text{1,3-bisphosphoglycerate} + \text{ADP} \rightleftharpoons \text{glycerate 3-phosphate} + \text{ATP}. \quad (1)$$

Yeast PGK has a weight of about 45 kDa and is composed of two domains which are connected by a well conserved hinge region where the catalytic reactions take place. Several of the studies cited above have been performed with the particular goal to better understand the role of the inter-domain motions for the function of the enzyme [4, 6, 7, 9]. A powerful space and time-resolved method for this purpose is neutron spin echo (NSE) spectroscopy, which has been used in Ref. [7] in combination with small-angle neutron scattering (SANS) and normal mode analysis and in Ref.[9] in combination with MD simulation. Standard NSE probes the slow motions and global diffusion of proteins on a 0.1-100 ns time scale and on a nm length scale. The results of the NSE studies suggest that the hinge-bending motions of the two domains in PGK enable its enzymatic activity and that the presence of the substrates rigidifies the molecular and accelerates its internal dynamics.

*E-mail: a.stadler@fz-juelich.de

†E-mail: gerald.kneller@cnrs.fr

The present article aims at extending and consolidating the abovementioned work with an analysis of QENS data from the high-resolution spectrometer IN16B at the Institut Laue-Langevin in Grenoble. The instrument probes the ns time scale if operated in BATS mode (backscattering and time of flight spectroscopy) [12] and closes the gap between QENS experiments with standard time-of-flight spectrometers and NSE spectroscopy.

The QENS experiments on PGK were performed at 283 K in presence and absence of the substrates (13mM MgATP, 41mM 3PG, 20 mM MOPS, 50 mM NaCl, 2 mM EDTA, pD 7.4, 99.9% atom D deuteriumoxide) using a PGK concentration of 50 mg/ml. PGK from yeast and all chemicals were obtained commercially from Sigma-Aldrich. These conditions are the same as in Ref. [7] and warrant that PGK in presence of substrates is more than 90% in the ligand-bound state. Prior to data analysis, the solvent-contributions were subtracted. Since about 50 % of the atoms in a protein are hydrogen atoms, which have a strongly dominant cross section for incoherent neutron scattering, the dynamic structure factor for QENS from PGK can be written in the form

$$S(\mathbf{q},\omega) = \frac{1}{2\pi}\int_{-\infty}^{+\infty} dt e^{-i\omega t} F(\mathbf{q},t), \quad (2)$$

$$F(\mathbf{q},t) \approx \frac{1}{N}\sum_{j\in\mathbb{H}} \left\langle e^{-i\mathbf{q}\cdot\hat{\mathbf{x}}_j(0)} e^{i\mathbf{q}\cdot\hat{\mathbf{x}}_j(t)} \right\rangle. \quad (3)$$

Here $\hat{\mathbf{x}}_j(t)$ is the time-dependent position operator of hydrogen atom j and the symbol $\langle\ldots\rangle$ denotes a quantum ensemble average, which leads to the the symmetry relations $F^*(\mathbf{q},t) = F(-\mathbf{q},-t)$ and $F(\mathbf{q},t) = F(-\mathbf{q},-t+i\beta\hbar)$.

As in several previous studies [13–16], the analysis of the QENS data has been performed in the time domain, employing a model for the symmetrized and resolution-deconvolved intermediate scattering function

$$F^{(+)}(\mathbf{q},t) = \frac{F(\mathbf{q},t+i\beta\hbar/2)}{F(\mathbf{q},i\beta\hbar/2)}. \quad (4)$$

Within Schofield's semiclassical approximation [17] $F^{(+)}(\mathbf{q},t)$ can be identified with the classical

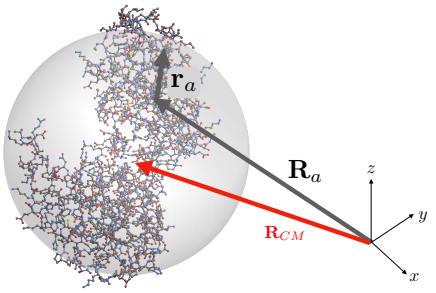

FIG. 1: The PGK molecule (PDB code 3PGK) together with a sphere of radius $R_H = 30.5\,\text{Å}$ which is used for the Stokes-Einstein relation (17) and the definitions of $\mathbf{R}_a$ and $\mathbf{r}_a$. The red arrow points to the center-of-mass.

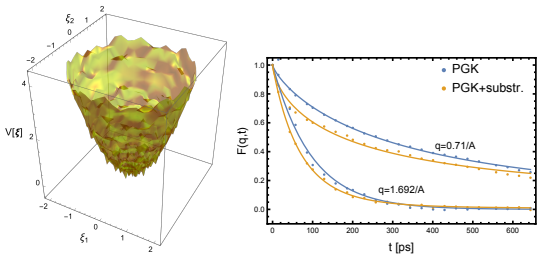

FIG. 2: **Left panel:** "Rough" parabolic potential. **Right panel:** Resolution-deconvolved $F(q,t)$ of PGK in deuterated solution without and in presence of substrates (blue and yellow dots, respectively) and the corresponding fits (blue and yellow line, respectively).

time correlation function, $F_{\text{cl}}(\mathbf{q},t) \equiv \lim_{\hbar\to 0} F(\mathbf{q},t)$, and the normalization factor in (4) ensures that $F^{(+)}(\mathbf{q},0) = 1$. For all the technical details of the data analysis, we refer to a recent QENS study of myelin basic protein on the same instrument [13].

For model building purposes, we assume that there is a representative hydrogen atom "a" whose dynamics accounts for both the relaxation dynamics of the individual hydrogen atoms and their motional heterogeneity. Within Schofield's semiclassical approximation we have then

$$F^{(+)}(\mathbf{q},t) \approx \left\langle e^{-i\mathbf{q}\cdot\hat{\mathbf{x}}_a(0)} e^{i\mathbf{q}\cdot\hat{\mathbf{x}}_a(t)} \right\rangle_{\text{cl}}, \qquad (5)$$

where $\langle\ldots\rangle_{\text{cl}}$ stands for a classical ensemble average. We assume furthermore that the domains in PGK can be treated as equivalent and that the motions of the scattering atom are uncorrelated with the motions of the domain to which it is attached. Writing $\mathbf{x}_a = \mathbf{R}_a + \mathbf{r}_a$, where $\mathbf{R}_a$ points to the center of the domain and $\mathbf{r}_a$ to the position of the scattering atom with respect to that reference point (see Fig. 1), the orientation-averaged intermediate scattering function of PGK in solution can then be factorized as

$$\overline{F}^{(+)}(q,t) \approx f(q,t)g(q,t) \qquad (q \equiv |\mathbf{q}|), \qquad (6)$$

where

$$f(q,t) \equiv \overline{\langle a^*_{\mathbf{q}} a_{\mathbf{q}}(t)\rangle_{\text{cl}}} \text{ and } g(q,t) \equiv \overline{\langle A^*_{\mathbf{q}} A_{\mathbf{q}}(t)\rangle_{\text{cl}}} \qquad (7)$$

are the orientation-averaged autocorrelation functions related to the respective dynamical variables

$$a_{\mathbf{q}} \equiv e^{i\mathbf{q}\cdot\mathbf{r}_a} \quad \text{and} \quad A_{\mathbf{q}} \equiv e^{i\mathbf{q}\cdot\mathbf{R}_a}. \qquad (8)$$

Introducing the generic variable (the $\mathbf{q}$-dependence is omitted)

$$\xi = \begin{cases} a_{\mathbf{q}} - \langle a_{\mathbf{q}}\rangle & \text{for intra-domain motions,} \\ A_{\mathbf{q}} - \langle A_{\mathbf{q}}\rangle & \text{for inter-domain motions,} \end{cases} \qquad (9)$$

the time evolution of both $f(q,t)$ and $g(q,t)$ can be described by the same dynamical model, requiring that nor $\langle a_{\mathbf{q}}\rangle$ neither $\langle A_{\mathbf{q}}\rangle$ vanish identically. In this case, the real and imaginary parts of ξ can be considered as independent dynamical variables and stochastic models can be used for the time evolution of the real two-component vector

$$\boldsymbol{\xi} \equiv \begin{pmatrix} \Re\{\xi\} \\ \Im\{\xi\} \end{pmatrix}.$$

We chose here the fractional Ornstein-Uhlenbeck process [18, 19], which describes anomalous, non-markovian diffusion in a harmonic bias potential,

$$V(\boldsymbol{\xi}) = \frac{K_\xi}{2}|\boldsymbol{\xi}|^2 \quad (K_\xi > 0),$$

which tends to restore the equilibrium configurations corresponding to $\langle\boldsymbol{\xi}\rangle = \mathbf{0}$. The force constant, K_ξ, has here the dimension of an energy and the fractional Fokker-Planck equation

$$\partial_t P = {}_0\partial_t^{1-\alpha}\left\{\eta_\xi^{(\alpha)}\frac{\partial}{\partial\boldsymbol{\xi}}\cdot\{\boldsymbol{\xi}P\} + D_\xi^{(\alpha)}\frac{\partial}{\partial\boldsymbol{\xi}}\cdot\frac{\partial P}{\partial\boldsymbol{\xi}}\right\}$$

describes the time evolution of the conditional probability $P(\boldsymbol{\xi},t|\boldsymbol{\xi}_0,0)$ for a transition $\boldsymbol{\xi}_0 \to \boldsymbol{\xi}$ within time t. Here $\eta_\xi^{(\alpha)}$ denotes a fractional relaxation constant, with physical dimension $1/\text{s}^\alpha$, and

$$D_\xi^{(\alpha)} = \eta_\xi^{(\alpha)} k_B T/K_\xi = \eta_\xi^{(\alpha)}\langle|\boldsymbol{\xi}|^2\rangle_{\text{cl}}$$

is a fractional diffusion coefficient. For $0 < \alpha < 1$ the fractional Riemann-Liouville derivative

$${}_0\partial_t^{1-\alpha} f(t) \equiv \frac{d}{dt}\int_0^t dt' \frac{(t-t')^{\alpha-1}}{\Gamma(\alpha)} f(t')$$

represents long-time memory effects and the normalized autocorrelation function (ACF) of $\boldsymbol{\xi}$ has the form of a stretched Mittag-Leffler (ML) function [20],

$$\phi(t) \equiv \langle\boldsymbol{\xi}(0)\cdot\boldsymbol{\xi}(t)\rangle/\langle|\boldsymbol{\xi}|^2\rangle = E_\alpha\left(-\eta_\xi^{(\alpha)}|t|^\alpha\right), \qquad (10)$$

which decays monotonously for $0 < \alpha \leq 1$ and displays a power law decay for large times,

$$E_\alpha\left(-\eta_\xi^{(\alpha)}|t|^\alpha\right) \overset{t\to\infty}{\sim} \frac{\eta_\xi^{(\alpha)} t^{-\alpha}}{\Gamma(1-\alpha)}. \qquad (11)$$

For $\alpha = 1$ the long-time tail disappears and $\phi(t)$ becomes an exponentially decaying function,

$$E_\alpha\left(-\eta_\xi^{(\alpha)}|t|^\alpha\right) \overset{\alpha\to 1}{=} \exp\left(-\eta_\xi|t|\right), \qquad (12)$$

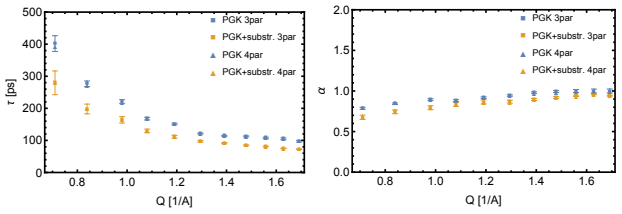

FIG. 3: The model parameters τ and α for PGK. Triangles indicate four-parameter fits (no error bars given) and squares three-parameter fits (with error bars). More explanations are given in the text.

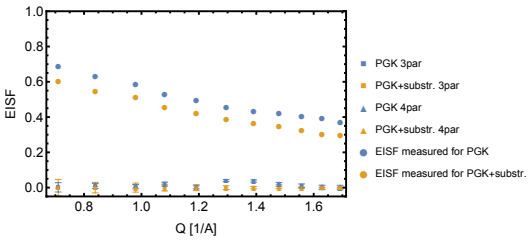

FIG. 4: The EISF parameter for PGK in absence and presence of substrates

where η_ξ has the dimension 1/s. The fOU process can be visualized as a diffusion process in the "rough" two-dimensional harmonic potential [21] which is depicted in the left panel of Fig. 2 and which is characterized by a wide distribution of energy barriers separating various minima or "conformational substates" [22]. We note here that the parameter α determines entirely the form of the distribution for the dimensionless barrier, $\epsilon = \Delta E/k_BT$, which reads [13]

$$P_{\mathrm{ML}}(\epsilon) = \frac{2\epsilon \sin(\pi\alpha)}{\pi\left(e^{-\alpha\epsilon^2} + e^{\alpha\epsilon^2} + 2\cos(\pi\alpha)\right)}. \qquad (13)$$

For $\alpha \to 1$ the barrier distribution is entirely concentrated on $\epsilon = 0$ and the "rough" harmonic potential becomes thus smooth. The corresponding diffusion process is the normal Ornstein-Uhlenbeck process [23], which leads to the exponentially decaying autocorrelation function (12). In the opposite case, $\alpha \to 0$, the distribution of energy barriers is flat, including also infinitely high barriers, and $\phi(q,t)$ exhibits a strongly non-exponential relaxation.

With these preliminaries and the definition $EISF(q) \equiv \overline{|\langle a_{\mathbf{q}}\rangle_{\mathrm{cl}}|^2}$ we arrive at the model [24]

$$f(q,t) \equiv EISF(q) + (1 - EISF(q)E_\alpha\left(-(|t|/\tau)^\alpha\right). \qquad (14)$$

for $f(q,t)$, where $EISF(q)$, $\tau \equiv \tau(q)$, and $\alpha \equiv \alpha(q)$ are the q-dependent fit parameters. Concerning the function $g(q,t)$, we assume that the time evolution of $A_{\mathbf{q}} - \langle A_{\mathbf{q}}\rangle$ is described by a normal OU process ($\alpha = 1$) and that $\overline{|\langle A_{\mathbf{q}}\rangle_{\mathrm{cl}}|^2} \approx 0$ in the fits. This leads to

$$g(q,t) \approx \exp\left(-D(q)q^2|t|\right), \qquad (15)$$

where the fit parameter, $D(q)$, has the dimension of a diffusion coefficient (m^2/s). For small q-values it follows from the cumulant expansion of the intermediate scattering function that

$$g(q,t) \overset{q\to 0}{=} e^{-\frac{q^2}{6}\langle(\mathbf{R}_a(t)-\mathbf{R}_a(0))^2\rangle} \overset{t\to\infty}{\sim} e^{-D_0 q^2 t}, \qquad (16)$$

where D_0 is the diffusion coefficient for a whole domain and thus for the whole PGK molecule.

We start the discussion of the results with the right panel of Fig. 2, which shows a fit of the resolution-deconvoloved intermediate scattering function, $\overline{F}^{(+)}(q,t) \approx f(q,t)g(q,t)$, with four parameters, $\tau(q)$, $\alpha(q)$, $EISF(q)$, and $D(q)$ for the minimum and maximum q-values in absence and presence of substrates. Fig. 3 displays the parameters τ (left panel) and α (right panel) as a function of q in presence and absence of the substrates (blue and yellow triangles, respectively) A clear impact of the presence of substrates on the intra-domain dynamics can be seen: Both τ and α are systematically reduced in presence of the substrates, which indicates that the internal molecular dynamics is accelerated by the enzymatic activity of the molecule and that the relaxation dynamics of the domains becomes less exponential. We note that τ and α in presence and absence of the substrates follow globally the same evolution with q. The time scale parameter τ becomes generally smaller with increasing q, which simply indicates that localized motions are faster than collective motions implying a large number of atoms. The form parameter, α, increases instead with q to values close to 1, indicating increasingly exponential relaxation for more localized motions. We attribute this behavior to the fact that less relaxation modes contribute to localized motions than to large amplitude motions which are probed at small values of q.

Fig. 4 presents the fitted EISFs together with the measured counterparts which are obtained by integrating the measured QENS intensity over the width of the resolution function. The details of the exact definition can be found in Ref. [16]. We find that the fitted EISF is globally close to zero in the presence and absence of the ligand, except at $q = 1.3\,\mathrm{Å}^{-1}$ where the EISF of PGK in absence of substrates ligand is slightly larger than the EISF in their presence. Correlating this observation with the decrease of α in presence of the substrates shows that the domains are slightly stiffened, which confirms again the findings in Ref [7] which were obtained by NSE spectroscopy. The dramatic difference between measured and fitted elastic intensities has been observed previously and can be attributed to spurious contributions of quasielastic scattering to the instrument-broadened elastic intensity [15]. For comparison we show also fits with a reduced model where $D(q) \equiv 0$ (blue and yellow squares, respectively). It can be clearly seen that the results are very similar, the difference being the error bars, which are much larger for the fit of all four parameters and which are not shown here. This observation is in line with the findings in Ref. [15] for the intrinsically disordered Myelin Basic Protein (MBP) and we present the three-parameter fits to show that the fits

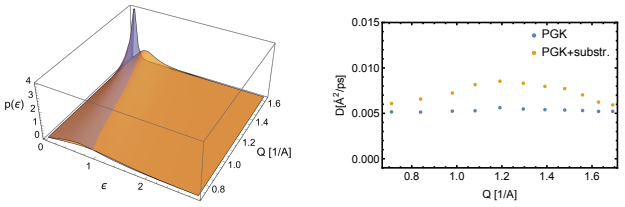

FIG. 5: **Left panel:** Energy barrier spectrum in absence (blue) and presence (red) of substrates. **Right panel:** The fitted diffusion coefficient $D(q)$.

of τ, α and $EISF$ are stable.

The impact of the enzymatic dynamics on the intra-domain energy landscape can be visualized by comparing the energy barrier profiles, $P_{\mathrm{ML}}(\epsilon)$, describing its "roughness" [13–15], which are displayed in the left panel of Fig. 5. Important differences between the two profiles are again observed for q-values corresponding to opening amplitudes of the hinge region and indicate a wider distribution of energy barriers in presence of the substrates. This corresponds to the decrease of the alpha parameter described above, indicating a stiffening of PGK in its active mode.

The q-dependent diffusion coefficient is displayed in the right panel of Fig. 5. One observes that $D(q)$ displays a pronounced modulation with respect to its values at small and large q-values. The latter are close to the estimation for the diffusion coefficient of a whole PGK molecule obtained from the Stokes-Einstein law,

$$D_0 = \frac{k_B T}{6\pi\eta R_H} \approx 5.1 \times 10^{-3} \text{Å}^2/\text{ps}. \qquad (17)$$

For this estimation we used an effective hydrodynamic radius of $R_H = 30.5\,\text{Å}$ calculated from the PDB structure 3PGK, including the diameter of a water molecule (see Fig.1). The maximum of $D(q)$ at about $q_{\max} = 1.2/\text{Å}$ corresponds to $2\pi/q_{\max} = 5.2\,\text{Å}$ in real space, which can be associated with breathing motions of the hinge-region in PGK caused by its enzymatic activity and which have also be observed by combining NSE spectroscopy and normal mode analysis [7]. The fact that $D(q) \approx D_0$ for smaller q-values is in line with the requirement that $g(q,t)$ must here describe diffusion of whole PGK molecules and $D(q) \approx D_0$ at higher q-values reflects that more localized motions do not affect the global diffusive dynamics of PGK.

To resume, we can say that our QENS study gives a consistent picture of the functional dynamics of PGK which confirms and completes an earlier study by NSE spectroscopy. It demonstrates in particular that the strongly non-exponential relaxation dynamics in proteins must be accounted for in the models used for the analysis of experimental data to fully exploit their rich information content.

ACKNOWLEDGMENTS: We gratefully acknowledge beam time allocation on the IN16B neutron spectrometer at the Institut Laue-Langevin, Grenoble, France (http://doi.ill.fr/10.5291/ILLDATA. 8-04-916). ANH acknowledges financial support from the Région Centre - Val de Loire and the Jülich Center for Neutron Scattering.

[1] P. Tanswell, E. W. Westhead, R. J. P. Williams, *European Journal of Biochemistry* **63**, 249 (1976).
[2] R. D. Banks, *et al.*, *Nature* **279**, 773 (1979).
[3] M. A. Sinev, O. I. Razgulyaev, M. Vas, A. A. Timchenko, O. B. Ptitsyn, *European Journal of Biochemistry* **180**, 61 (1989).
[4] B. E. Bernstein, P. A. M. Michels, W. G. J. Hol, *Nature* **385**, 275 (1997).
[5] E. Balog, *et al.*, *Physical Review Letters* **93**, 028103 (2004).
[6] Z. Palmai, *et al.*, *Proteins: Structure, Function, and Bioinformatics* **77**, 319 (2009).
[7] R. Inoue, *et al.*, *Biophysical Journal* **99**, 2309 (2010).
[8] E. Balog, D. Perahia, J. C. Smith, F. Merzel, *J Phys Chem B* **115**, 110510094236054 (2011).
[9] N. Smolin, R. Biehl, G. R. Kneller, D. Richter, J. C. Smith, *Biophysical Journal* **102**, 1108 (2012).
[10] X. Hu, *et al.*, *Nature Phys* **12**, 171 (2016).
[11] *The Enzymes. 8: Group Transfer. Part A: Nucleotidyl Transfer, Nucleosidyl Transfer, Acyl Transfer, Phosphoryl Transfer* (Acad. Pr, New York, 1973), third edn.
[12] M. Appel, B. Frick, A. Magerl, *Physica B: Condensed Matter* **562**, 6 (2019).
[13] M. Saouessi, J. Peters, G. R. Kneller, *J. Chem. Phys.* **150**, 161104 (2019).
[14] M. Saouessi, J. Peters, G. R. Kneller, *J. Chem. Phys.* **151**, 125103 (2019).
[15] A. N. Hassani, *et al.*, *The Journal of Chemical Physics* **156**, 025102 (2022).
[16] A. N. Hassani, A. M. Stadler, G. R. Kneller, *The Journal of Chemical Physics* **157**, 134103 (2022).
[17] P. Schofield, *Physical Review Letters* **4**, 239 (1960).
[18] R. Metzler, J. Klafter, *Phys Rep* **339**, 1 (2000).
[19] R. Metzler, J. H. Jeon, A. G. Cherstvy, *Phys Chem Chem Phys* **16**, 24128 (2014).
[20] R. Gorenflo, A. A. Kilbas, F. Mainardi, S. V. Rogosin, eds., *Mittag-Leffler Functions, Related Topics and Applications*, Springer Monographs in Mathematics (Springer, Heidelberg, 2014).
[21] R. Zwanzig, *Proceedings of the National Academy of Sciences* **85**, 2029 (1988).
[22] H. Frauenfelder, S. G. Sligar, P. G. Wolynes, *Science* **254**, 1598 (1991).
[23] G. Uhlenbeck, L. Ornstein, *Physical Review* **36**, 823 (1930).
[24] G. R. Kneller, *Proceedings of the National Academy of Sciences* **115**, 9450 (2018).